Wet foam flow: A suitable method for improving surface hygiene in the food industry

Heni Dallagi, Christine Faille, Laurent Bouvier, Maureen Deleplace, Thomas Dubois, Fethi Aloui, Thierry Benezech

1   Wet foam flow: a suitable method for improving surface hygiene in the food industry

2

3   Heni DALLAGI[a], Christine FAILLE[a], Laurent BOUVIER[a], Maureen DELEPLACE[a], Thomas DUBOIS[a], Fethi

4   ALOUI[b], Thierry BENEZECH[a]*

5

6   [a] Univ. Lille, CNRS, INRAE, Centrale Lille, UMET, F-59000 Lille, France

7   [b] Polytechnic University Hauts-de-France, LAMIH CNRS UMR 8201, Campus Mont-Houy, F-59313

8   Valenciennes, France

9

10   **Corresponding Author:** Thierry BENEZECH, INRAE, UMET, 369 rue Jules Guesde, F-59650 Villeneuve

11   d'Ascq, France. thierry.benezech@inrae.fr

12

13

14

15

ABSTRACT

In the food industry, the cleaning of contaminated surfaces requires new strategies to be adopted which can provide greater cleaning efficiency with minimal energy and water consumption. The use of wet foams was proposed to clean stainless steel surfaces contaminated by droplets containing *Bacillus* spores. Methods such as polarography, conductimetry and foam structure identification were used. Foam flow conditions with varying wall shear stresses and bubble sizes were observed to measure their impacts on surface contaminant removal kinetics. Compared to conventional cleaning-in-place method, foam flow more effectively removed both hydrophilic and hydrophobic spores. The combination of high shear stress and small bubble sizes (<0.2 mm) showed promise for improving the cleaning efficiency of the foam. Mechanisms such as fluctuation in local stresses, or in the liquid film thickness between the bubbles and the steel wall induced by bubble passage, foam imbibition and liquid film drainage were then investigated.

42

1. Introduction

In the agro-food industrial environment, avoiding surface contamination by unwanted microorganisms is of crucial importance (Alvarez-Ordonez et al., 2019; Farag et al., 2021). Indeed, contaminated surfaces can recontaminate food in contact (cross-contamination), with sometimes disastrous consequences in terms of food spoilage, but also in terms of transmission of pathogens that can be the cause of large-scale epidemics. For example, surface contamination with microorganisms would have accounted for more than 50% of the collective foodborne illnesses (CFTI) in France between 2006 and 2008 (Delmas et al., 2010). Nowadays, cleaning-in-place (CIP) is a routine method in the food and pharmaceutical industries to ensure the equipment hygiene and the quality of product. The effect of the hydrodynamics of the cleaning fluid on CIP efficiency has been the subject of numerous studies (Li et al., 2019; Piepiórka-Stepuk et al., 2021). Particular interest has been shown in parameters such as the mechanical action exerted by the flow in creating wall shear stress (Bénézech and Faille, 2018) or the impact of Reynolds number (Fan et al., 2018). Their results showed that turbulence affects the cleaning process, as an increase in the presence of turbulent structures generated at the walls could improve the cleaning efficiency, but up to a certain limit. The use of non-stationary flows, such as pulsed flows and intermittent jet flows, would appear to increase CIP efficiency. Indeed, these kinds of flows affect both the mean and fluctuating components of the wall shear stress and consequently reduce the residual contamination (Absi and Azouani, 2018; Blel et al., 2013).

Gas-liquid two-phase flows (air bubbles in liquid or foam), which are also non-stationary flows, are likely to be of similar interest to pulsed flows. Indeed, liquid containing gas bubbles (non-foaming solution) had been shown to efficiently remove from surfaces both particles (Kondjoyan et al., 2009) and bacteria (Kriegel and Ducker, 2019). Recently, the efficiency of foam flow to remove *Bacillus* spores from stainless steel surfaces has been investigated by (Al Saabi et al., 2021) and the use of

68   aqueous unstable foams has also been proposed for cleaning the sensitive surfaces of artistic and

69   cultural assets (Schad et al., 2021). It should also be noted that foam in static conditions, is widely

70   used in the food industry for cleaning open surfaces (floors, conveyor belts, worktops and

71   equipment) (Mierzejewska et al., 2014).

72   Aqueous foam could be considered as a non-Newtonian fluid consisting of gas dispersion in liquid

73   containing surfactants. Depending mainly on the liquid fraction, the foam could be ranked as wet

74   (small and spherical bubbles) or dry (large and polyhedral bubbles). A liquid-rich layer may be formed

75   near a solid surface due to the bubble migration, thereby giving a slip effect between the foam and

76   the wall (Tisné et al., 2003). Given this complexity, the rheological behavior of foam can follow the

77   shear-thinning Herschel-Bulkley model, which states that under strong mechanical stresses, foam

78   behaves as a viscous liquid, while under low stresses it behaves as a solid whose structure can be

79   deformed and return to its initial state (Dallagi et al., 2019). Moreover, very wet foam flow (liquid

80   fraction = 0.5) was found to clean hydrophilic spores better than dryer foam (liquid fraction between

81   0.3 to 0.4) (Al Saabi et al., 2021). However, the maximum of the shear stress that they used was 6 Pa,

82   and the work lacks the explanation of the cleaning process.

83   The aim of this study was to investigate the potential role of the foam velocity and their structure

84   (described by air/water content of the foam and size of air bubbles) in efficiently removing Bacillus

85   subtilis spores. In this respect, different flow conditions of wet foam (liquid fraction = 0.5), by varying

86   the shear stress (from 2 up to 13.2 Pa) and the foam structure, were carried out to test its efficiency.

87   All cleaning conditions were tested on two *Bacillus* spore strains which differ only in their

88   hydrophilic/hydrophobic character. Another originality of this present work is the detailed physical

89   analysis of the dynamic behavior of foam and its structure and consequences at the wall to identify

90   the underlying mechanisms of the bacterial spores' removal and choose the foam flow condition

91   leading to optimal cleaning. The foam cleaning effectiveness was then compared to a standard CIP

92   procedure.

93

94 ## 2. Materials and Methods

95 ### 2.1. Foam preparation

96   The foam production prototype was built according to a previous work (Al Saabi et al., 2021). The

97 prototype is presented in Fig. 1. Briefly, foam was produced by pressurized air injection through a

98 porous medium (pore sizes ranging from 1 to 1.6 µm) into an SDS surfactant (Sodium Dodecyl Sulfate

99 (over 98.5% purity) dissolved in osmosed water (0.15% w/w) to avoid any unwanted interactions

100 with ions contained in the standard tap water.

101   The physical properties of the foaming solutions used were a 1 Bar atmospheric pressure and

102 20°C standard temperature, a 997.9 kg/m^3 density (ρ_l), a 0.94 10^{-3} Pa.s dynamic viscosity (μ_l) and a

103 26.2 10^{-3} N/m surface tension (σ). The foam quality (β) describing the air/water content of the foam

104 was calculated as follows (Equation 1) where Q_g and Q_l are respectively the gas and liquid flow rates.

105 $$\beta = \frac{Q_g}{Q_l + Q_g}$$ (1)

106   A foam quality of 0.5 was chosen in this work by varying the shear stress and the capillary forces.

107 The capillary force of the bubble $F_c = \sigma 2\pi r$ is defined as the force due to surface tension that acts

108 between the two halves of the bubble (Al-Qararah et al., 2013) with respect to the capillary pressure

109 ($P_c = \frac{\sigma}{r}$) (Schad et al., 2021), where r is the bubble radius. The balance between the viscous drag

110 forces versus surface tension forces of the foam can be represented by the non-dimensional capillary

111 number $Ca = \frac{\mu_l v}{\sigma}$. μ_l and v are the dynamic viscosity of the liquid solution and the foam velocity,

112 respectively.

113   Therefore, the first part presents a detailed characterization of these foam flow conditions in

114 order to understand the mechanism by which the foam detached the spores, to identify the key

115 parameters and then to test these new foam conditions on cleaning of stainless-steel coupons

116 contaminated by *Bacillus* spores. Table 1 (in Result section) summarizes all the FFC conditions

117 (quality of 0.5) and CIP. The foam mean velocity ($\bar{v}$) and the Reynolds number (Re) are determined

118 from the following equations:

119    $Re = \frac{\rho_f.\bar{v}.d_h}{\mu_f}$ d_h being the hydraulic diameter   (2)

120    $\bar{v} = \frac{Q_l + Q_g}{S}$ S being the duct section   (3)

121    $\rho_f = (1-\beta).\rho_l + \beta.\rho_g$ ρ_l being the liquid density   (4)

122    $\mu_f = \frac{\mu_l}{1-\mu_l^{1/3}}$ (5)

123   The foam flow conditions varied from 1.5 to 13.5 cm/s (Q_g= Q_l; are 4.5, 9, 13.5, 27, and 40.5 l/h

124   for the cases 1, 2, 3, 4, and 5 respectively). The three first cases correspond to the conditions used in

125   a previous work (Al Saabi et al., 2021). Cases 4 and 5 have the highest velocities, which were

126   generated using three parallel generators. CIP has the highest velocity, while the mean shear stress

127   was similar to that in case 4.

128

129   **2.2. Foam characterization**

130   2.2.1.   Foam morphology

131   Foam flow was visualized in order to observe the bubble's displacement at the channel walls, for

132   a given interval. A Nikon D850camera, equipped with an AF-S Micro NIKKOR 60 mm f/2.8 G ED with a

133   resolution of 8256 x 5504 pixels, was used to record foam microtexture and its associated bubble size

134   distribution. For each foam flow condition, three images were captured then analyzed using

135   Piximètre 5.1 R1540 software. First, the chosen images were calibrated, then were subjected to

136   different image processing features (local threshold, filters…) to reduce the noise in order to better

137   observe its contours. The bubble size distribution was then calculated according to usual

138   granulometric distributions. To evaluate the heterogeneity/uniformity of this distribution, different

139   parameters were identified such as *F0.05*, and *F0.2* corresponding to the percentage of the bubbles

140   with a diameter of less than 0.05 and 0.2 mm respectively.

141   2.2.2.   Thin film thickness

142   The conductimetry technique was used to measure the thickness of the thin film. This is based on

143   the measurement of the impedance of the liquid volume located between the liquid-foam interface

144 and two outcropping electrodes at the duct wall. A generator provided an alternating sinusoidal

145 voltage to power these electrodes. The frequency was 50 kHz to avoid any polarization phenomena.

146 The calibration of the conductimetric probe was carried on using the calibrated Mylar sheets. The

147 estimated error was 8%.

148 2.2.3.   Wall shear stress

149   When foam flowed, mean shear stress was calculated based on the measurement of the static

150 pressure along the channel. The power loss measurements were carried out using a differential

151 pressure sensor Shlumberger, type 8D. Two pressure outlets allow the connection of 2 manifold

152 tubes placed over a scaled plate that measures on a length L of 1m the pressure drop placed after 1.5

153 m from the entry of the foam in the duct. Indeed, to allow steady state flow conditions, the test

154 ducts were placed at intervals exceeding 80 times the hydraulic diameter of the vein inlet (i.e. 1.5 m).

155 The mean wall shear stress can thus be computed as:

156 $\bar{\tau} = \frac{\Delta P}{\Delta x} \frac{d_h}{4}$ (6)

157 where $\frac{\Delta P}{\Delta x}$ is the pressure gradient.

158   The local shear stress at the top wall where coupons were placed, was measured using the

159 polarography method. This technique allows the determination of the local velocity gradient at the

160 walls by measuring the mass transfer coefficient of the electrodes. Briefly, based on the simplified

161 assumptions for the resolution of the convection-diffusion equation proposed by (Mitchell, 1965),

162 the wall shear stress calculation was obtained from the velocity gradient (Lévêque solution and

163 Sobolic correction). Details of the method used here were given previously (Tisné et al., 2003).

164   From a theoretical point of view, the polarographic signal is related to the slip layer thickness and

165 foam velocities. The diffusion limit current can be represented as the Sherwood number form (*Sh*) or

166 directly as the wall shear stress (τ_w). Spectral analysis of the time signals appears necessary in order

167 to understand the underlying mechanisms and to trace back to the flow characteristics near the wall

168 duct. The method used for spectral representation is based on the processing of the signal acquired

169 by the Fourier transform (*FT*) with Matlab software. This was proposed by (Ioana et al., 2007). It

170 expresses the frequency distribution of the amplitude, the power spectral density, as well as the

171 fluctuation rate of the considered signals. These specters revealed peaks obtained at characteristic

172 frequencies corresponding to the passage frequencies of bubbles respective to each foam condition

173 and their harmonics.

174   It was found that the SDS did not support the addition of electrochemical products (Ferri-

175 ferrocyanide potassium) for the use of the polarography method. In fact, a reaction other than

176 oxidation-reduction was produced, destabilizing the foam. For this reason, we replaced the SDS with

177 a non-anionic surfactant: Lauramine oxides (Ammonyx® LO (Stephan) = 0.8 ml/l). To ensure the

178 presence of the same phenomena for the same flow conditions, the thickness of the liquid film and

179 of the conductivity signals produced with that of the SDS solution was verified. The same behavior

180 and signal variation with SDS or Ammonyx® surfactant was observed, which is in line with previous

181 works (Tisné et al., 2003), where another surfactant (Amonyl®) replaced the SDS for the same reason.

182

183 **2.3. Bacterial strains and materials**

184   Two *Bacillus subtilis* strains were used throughout this study. *Bacillus subtilis* PY79 (subsequently

185 named Bs PY79) is a laboratory strain producing hydrophilic spores surrounded by a mucous layer

186 called crust. A Bs PY79 recombinant strain deleted in *spsA* (Dubois et al., 2020), subsequently named

187 Bs PY79 *spsA*, which produces hydrophobic spores modified in their crust properties, was also used

188 throughout this study. Both *Bacillus* strains were tagged with green fluorescent proteins to make the

189 spores more fluorescent. Spores were produced as previously described (Faille et al., 2019) on Spo8-

190 agar at 30°C. When over 95% of spores were obtained, they were harvested by scraping the surface,

191 washed five times in sterile water, and stored in sterile water at 4°C until use. In order to limit the

192 presence of spore aggregates, the spore suspensions were subjected to an ultrasonication step

193 (Bransonic 2510E-MT, Branson Ultrasonics Corporation, USA) before each experiment.

194   All experiments were carried out on AISI 316 stainless steel with pickled (2B) finish coupons

195 (provided by APERAM, Isbergues, France) in the form of rectangular coupons (45 mm × 15 mm). In

196   order to have surface properties similar to those used in the dairy industry, the stainless-steel

197   coupons were subjected to a conditioning procedure consisting of 15 runs of soiling and cleaning

198   both to mimic what might occur in food processing lines and to stabilize their surface properties. The

199   soiling step was achieved by immersing the coupons in milk in semi-skimmed reconstituted milk (150

200   g/l milk powder) for 30 min at room temperature. After a quick rinse, soiled coupons were cleaned

201   by immersion in sodium hydroxide at 0.5% w/w for 30 min at 70°C. Before each experiment, coupons

202   were cleaned using an alkaline detergent (RBS T105, Traitements Chimiques des Surfaces, France).

203   Each coupon was first rubbed vigorously with pure RBS and then immersed for 10 minutes in 5% RBS

204   at 60°C. Coupons are thoroughly rinsed for 5 min with tap water, and then with softened (reverse

205   osmosis) water for another 5 min. One day before experiments, coupons were sterilized in a dry heat

206   oven at 180°C for 1h.

207   The hydrophilic character of the cleaned and disinfected coupons was estimated using a

208   goniometer (Digidrop, GBX, France). A water contact angle (θ_{water}) of 66° was measured, which

209   reflects the relatively hydrophilic character of this material.

210

211   **2.4. Surface soiling and cleaning**

212   For both strains, the concentration of the spore suspensions was set at 10^8 CFU/ml. Five 1 µl

213   droplets of the spore suspension were placed on each coupon and evaporated for 1h at 30°C. The

214   procedure was schematically illustrated Fig. S1. Some coupons were analyzed to control the initial

215   contamination level (5 10^5 spores per coupon) and to observe the droplet architecture under the

216   microscope (Fig. S1 in the Supporting Information). Then, sets of 4 coupons were placed inside a

217   rectangular stainless-steel duct (1.5 10^{-2}m high × 1 10^{-2}m width), subjected to a cleaning procedure

218   and analyzed again for residual contamination (three coupons) for enumeration and deposit

219   architecture (one coupon).

220   In this work, as previously (Al Saabi et al., 2021), the foam cleaning phenomenon was evaluated

221   at the top wall because the wall shear stress and the thin liquid film thickness would be considered to

222 show constant variations in this zone according to previous work (Tisné et al., 2004, 2003). This

223 position was selected in order to facilitate the interpretation of the role of foam flow in the cleaning

224 process.

225

226 The resistance of the spore deposits to a cleaning procedure was performed as follows. The test

227 ducts were connected to the pilot rig and then were subjected to the cleaning process. Experiments

228 were carried out on foam flow cleaning (FFC) under different conditions (by varying the foam shear

229 stress and the foam/bubble structure) for 15 and 35 s, 1, 3, 5, 10, and 20 min. Other experiments

230 were carried out on cleaning in place (CIP) under the same conditions to compare the relative

231 effectiveness of FFC and CIP. Details are provided in the Results section. After the cleaning process,

232 the coupons were removed from the test duct, then rinsed by immersion in sterile ultrapure water to

233 remove the rest of the foam. In order to investigate the possible role of the presence of SDS

234 surfactant on spore detachment, further experiments were performed in static conditions by dipping

235 a set of coupons in pure water or in SDS 0.15% (w/w) for 20 min (data not shown). It should be noted

236 that Bs spore incubation in SDS did not result in any significant viability loss.

237 To determine the quantity of spores on the coupons before and after cleaning, each coupon

238 surface was sampled using a dry cotton swab (Copan, Brescia, Italy). The swabs were placed in a tube

239 containing 5 ml of sterile ultrapure water and vortexed for 1 min at 2400 rpm. The suspensions

240 containing the detached spores were enumerated on TSA (Tryptone Soy Agar, Biokar, France) after

241 48h at 30°C. For microstructure examination, the observation of some deposits was performed

242 before and after cleaning, using an epifluorescence microscope (Zeiss Axioskop 2 Plus, Oberkochen,

243 Germany). The observations were first made at low magnification (x50) in order to observe the

244 whole deposit resulting from the drying of a droplet. Further observations were carried out at higher

245 magnification (x400) to determine the fine structure of the densest parts of these deposits (clusters,

246 peripheral rings…), including any 3D organization.

247 After cleaning, the deposits were mostly weakly fluorescent, which made them difficult to

248 observe. It was therefore necessary to stain them before observation. For that purpose, dried

249 coupons were stained with orange acridine (0.01%) for 15 min. In order to ensure that the deposits

250 were not removed during this staining step, some deposits were observed before and after the

251 staining step. No significant difference was observed.

252

253

254 **2.5. Kinetics modeling**

255 The removal kinetic profiles of the percentage of residual spores were fitted according to

256 previous work (Bénézech and Faille, 2018), using GInaFIT. A two-phase model was selected (Equation

257 7), which presents the existence of two subpopulations characterized by different removal behaviors.

258 $\frac{N}{N_0} = f\, e^{(-k_{max1}t)} + (1-f)e^{(-k_{max2}t)}$ (7)

259 Where N_0 is the initial bacteria count, f is the poorly adherent fraction of the population (less

260 resistant to detachment), ($1-f$) is the more adherent fraction, and k_{max1} and k_{max2} [s^{-1}] are the specific

261 detachment rates of the two sub-populations.

262

263 **2.6. Statistical analysis**

264 All the experiments were carried out in triplicate. Statistical analyses were performed by general

265 linear model procedures using SAS V8.0 software (SAS Institute, Gary, NC, USA). For each cleaning

266 condition, variance analyses were performed to determine the possible role of the shear stress and

267 the foam structure on the removal kinetics of spores (f, k_{max1}, and k_{max2}) and the effectiveness of the

268 cleaning by foam flow compared to the CIP process.

269

270 **3. Results**

271 In this study on the detachment of adherent spores by foam, it was essential to dispose of a

272 procedure allowing very reproducible contamination of the surfaces, both in terms of contamination

273   rates and in terms of the structure of the deposits. For this reason, we chose to contaminate the

274   materials with droplets containing *Bacillus* spores and to let these deposits dry as previously

275   described (Deleplace et al., 2021). For the type of foam (more or less dry), we chose to use a so-

276   called wet foam (foam quality of 0.5) because recently published work had shown that dryer foams

277   (liquid fraction from 0.4 to 0.3) were less effective (Al Saabi et al., 2021). We used SDS as model

278   surfactant system to produce the foam. In order to identify the key parameters affecting the

279   efficiency of foam cleaning, we first performed a series of physical measurements of foams obtained

280   under different conditions, and we measured the effect of these parameters on the cleaning

281   efficiency in terms of spores' detachment during cleaning procedure and patterns deposition after

282   cleaning.

283

284   **3.1. Foam flow characterization**

285   ***3.1.1.   Bubbles size distributions***

286   Fig. 2 shows top views of the foam at the top wall for the different flow conditions. For all foam

287   flow conditions, the bubbles had a roughly spherical shape and were separated by thick liquid films

288   (lamellae). Different foam morphologies were observed. Indeed, when the velocity increased from

289   1.5 to 9 cm/s, a clear decrease in the bubble size was observed. However, no additional decrease

290   could be observed between 9 and 13.5 cm/s. Bubble sizes were then measured for these different

291   conditions and the curves of the cumulative fraction of the bubble size distributions are presented in

292   Fig. 3. First, the distribution of the bubble size in all conditions was fitted by a lognormal function (R^2

293   ranging from 0.89 to 0.97) to better visualize the differences between the conditions tested.

294   Variation of velocity causes a change in foam structure and bubble size distribution. As the foam

295   velocity increased (Table 1), the mean diameter of bubbles decreased (from 0.34 down to 0.18 mm,

296   for foam at 1.5 and 9 cm/s respectively) and the distribution became more homogeneous, except for

297   foam at 13.5 cm/s where the mean diameter was 0.21 mm. While the number of small bubbles (less

298   than 0.05 mm in diameter) was very close at 9 and 13.5 cm/s, intermediate-sized bubbles (between

299   0.2 and 0.6 mm in diameter) were more abundant at 9 cm/s than at 13.5 cm/s. Therefore, the

300   cumulative bubble size number at 0.2 mm (*F02*) was 0.68 and 0.60 respectively for 9 and 13.5 cm/s,

301   as indicated in Table 1 and were found to be statistically different (Pr < 0.0001). These differences

302   were much greater when comparing the highest velocities to the lowest ones. Indeed, considering

303   bubbles with a diameter ≤ 0.05 mm (see fraction *F005*, Table 1), at 13.5 cm/s the cumulative fraction

304   was more than 20 times higher than that for the lowest foam velocities, at 1.5 cm/s.

305   ### 3.1.2.   Upper liquid film thickness

306   Foam is not in direct contact with the wall surface, but bubbles are slipping over a thin liquid film

307   layer (a few micrometers width). Variations of the liquid film thickness (from 11 up to 13 μm)

308   measured at the top wall are shown in Fig. 4 (left) for three foam mean velocities of 1.5, 3, and 4.5

309   cm/s, bearing in mind the limitations of our experimental set-up essentially due to the inability to

310   access sufficiently high foam flow rates as it was possible for the cleaning experiments. The film

311   thickness was affected by the bubble passage as shown in Fig. 4 (left) with an example of the

312   observed temporal evolution of the signal at the middle of the test section. It should be noted that

313   whatever the position of the probe the signal was observed as similar either on the sides or in the

314   middle of the duct. In the three cases, conductimetry signals presented high fluctuations reflecting

315   the non-uniformity of this liquid film. Indeed the signals showed an instantaneous variation of 72 and

316   54% relative to the mean thickness value which varied from 5 to 21 μm, and from 8 to 22 μm for

317   foam at 1.5 and 4.5 cm/s, respectively. In addition, the profiles obtained appeared to be very

318   different within the three cases. The higher is the velocity the higher is the frequency of the signal

319   (variation from 45 to 72.5 Hz for cases of foam at 1.5 and 4.5 cm/s, respectively), and the lower is the

320   amplitude (variation from 9.8 up to 6 μm, respectively). These variations were directly linked to the

321   frequency of passage of the bubbles and to the size variations leading to the shape of the signal.

322   Indeed, the maximum thickness of the liquid film (peaks of the signal) corresponds to the film

323   thickness between two following bubbles passage, minimum thickness (signal hollows)

324   corresponding to the presence of the bubble, the bigger bubble the lower film thickness could be

325 stated from Fig. 2. It should be noted that conductimetry results, for both tested surfactants SDS and

326 Ammonyx, have shown the same instantaneous evolution and presented the same phenomena at

327 the walls. A variation of 61 and 42% relative to the mean thickness and an increase of frequency from

328 37.5 to 77.5 Hz for cases of foam at 1.5 and 4.5 cm/s respectively, are shown in Fig. S2 in the

329 Supporting Information.

3.1.3. Wall shear stress

331 To highlight the effect of the passage of a bubble on the shear rate at the wall, temporal signals

332 from the frequency response of the polarography probe located in the middle of the channel have

333 been plotted (Fig. 4, right).

334 The wall shear stresses on the upper region of the duct appeared larger and approximately

335 double the value of the average stress measured on the section (data not shown). This is in relation

336 to the low thickness of the liquid film at this location. The average shear stress increases slower than

337 the foam flow velocity but increases from 4.3 Pa at 1.5 cm/s to 7.2 and 8.1 Pa for velocities of 3 and

338 4.5 cm/s, respectively. More interesting were the temporal variations of the wall shear stress at the

339 top wall as shown in Fig. 4 (right), the signal varies periodically with a more homogeneous pattern

340 with velocity increase but a decrease in amplitude is clearly visible at 4.5 cm/s. The rate of fluctuation

341 of the wall shear (*RFS*) related to the signal amplitude decreases as the foam velocity increases

342 reaching 957, 688, and 491% for the three foam velocities tested, 1.5, 3, and 4.5 cm/s respectively.

343 The passage of bubbles, as seen in the film thickness variations, causes these variations in local shear

344 stress. These fluctuations are therefore characterized by a frequency that corresponds directly to the

345 frequency of bubble sliding on the upper wall.

346 Observing the spectral densities of the wall velocity gradient, all the curves had almost the same

347 shape of which spectrums obtained with the probes gave a low energy level (Fig. S3 in the Supporting

348 Information). The frequencies of bubbles are 20, 39, and 45 Hz for the first three cases respectively.

349 For the other foam conditions, the frequency and the *RFS* were determined by the extrapolation of

350 these experimental results and the theoretical correlations between the frequency and foam

351   parameters (where $f_{bi} = \frac{\beta.v}{d_{bi}}$, $A_{bi} = \frac{v}{f_{bi}}$, and d_{bi} are the frequency, amplitude, and diameter of i

352   bubble). As was expected, foam at higher velocities (9 and 13.5 cm/s) had the highest frequency (76

353   Hz) with a strong decrease in the wall shear fluctuation rate (130% for foam at 9 cm/s) (Table 1). All

354   results are reported in Table 1.

355

356   **3.2. Spores' detachment**

357   ***3.2.1.   Resistance to cleaning procedures***

358   The cleaning kinetics for the two bacterial spores are presented in Fig. 5 based on the evolution

359   of the mean values of the logarithmic reduction of adherent spores with the cleaning time. In all

360   cases, the detachment curves clearly showed two distinct phases. Both phases appeared to be

361   exponential and therefore were quite accurately described by the biphasic model, with R^2 ranging

362   from 0.84 to 0.97. Whatever the flow conditions, the first detachment phase lasted less than 1 min,

363   and the duration of this phase depended on the flow conditions of the foam (shorter at low velocity,

364   for the two spores), but especially on the strain. At 1 min, the resulting log reduction of the adherent

365   spores during this first phase ranged between 1.94 and 2.6, and between 0.95 and 1.33 for Bs PY79

366   and Bs PY79 *spsA*, respectively. The second phase was much longer and would probably continue

367   over 20 min. The detachment rate of the hydrophilic spores (Bs PY79) during this second phase was

368   quite low at 1.5, 4.5, and 13.5 cm/s resulting in an additional 0.15-0.28 log reduction of the adherent

369   spores, whereas at 9 cm/s the reduction reached around 1.15 log. A similar trend was observed for

370   the hydrophobic spores with 0.2-0.3 log reduction at 1.5, 4.5, and 13.5 cm/s and 0.45-0.57 log

371   reduction at 9, and 13.5 cm/s.

372   The role of the flow parameters and strains on the three kinetics parameters (f, k_{max1}, and k_{max2})

373   was then investigated. When comparing the two strains, the influence of the strains on the removal

374   efficiency during the first phase represented by the two parameters f (poorly adherent fraction of the

375   population) and k_{max1} (first kinetics constant rate) was highly significant as confirmed by the variance

376   analysis (Pr < 0.0001 for both parameters). According to Tukey's groupings, f was significantly

377   affected by the strain, with mean values of 0.92 and 0.998 for Bs PY79 *spsA* and Bs PY79 respectively

378   as shown in Fig. 6. The initial detachment rate (k_{max1}) also was largely dependent on the strain (from

379   1.7 up to 3.4 times higher for hydrophilic spores), while the second detachment rate (k_{max2}) was not

380   affected and was quite similar for the two strains (Fig. 6, no significant differences).

381   The role of the flow parameters as the shear stress (mean value, frequency, and *RFS*) and/or to

382   the distribution of bubbles (mean diameter and *FO2*) on the three kinetics parameters (*f*, k_{max1}, and

383   k_{max2}) was then investigated (Table 2 and Fig. 7). Whatever the parameter in relation to the flow and

384   the bubble size arrangement the Tukey's grouping tests gave the same ranking between the 4

385   velocities tested (Table 2) and can be visualized clearly in Fig. 7, the two groups of parameters as the

386   ones related to the wall shear stress and the ones related to the bubbles' size influencing, in the

387   same way, the removal kinetics. However, differences between the two strains could be stated. For

388   Bs PY79, the first kinetics phase rate constant k_{max1} was similar for all the studied cases (no difference

389   according to the Tukey' test) but an effect was observed on *f* with a significant difference between

390   the lowest and the highest velocities (1.5 and 4.5 compared to 9 and 13.5 cm/s) leading however to

391   an improvement while increasing the mean shear stress (Fig. 7, black dots). Conversely, k_{max2} was

392   significantly higher in the case of foam at 9 cm/s comparatively to the other cases whatever the

393   strains. Some differences could be seen with the hydrophilic spores, according to Tukey's grouping in

394   Table 2 and Fig. 7, red dots.   Indeed, the maximum foam velocity tested induced a significantly

395   higher value of *f* (Pr < 0.0001), a phenomenon more marked than with hydrophilic spores, as for

396   k_{max1}, it was significantly higher at this velocity than at the lowest velocity tested (Pr < 0.013).

397   However, k_{max2} variation trend with the velocity was similar to those of the hydrophilic strain and also

398   highly significant (Pr < 0.0007), the velocity of 9 cm/s being the best option. It should be noted that it

399   was not the highest mean shear stress tested (13.2 Pa), but it has the lowest bubble sizes (mean

400   diameter of 0.18 mm and *FO2* of 0.68).

401   Cleaning with foam was then compared to a CIP procedure (pink and black curves in Fig. 5) using

402   the SDS solution at a shear stress of 9.8 Pa, shown to be the most efficient condition with foam.

403   Concerning hydrophilic spores, the first detachment's phase in the case of CIP was shorter than for

404   foam cleaning and the removal was 0.5 log CFU less efficient. In addition, very few spores were

405   detached in the second phase, resulting in about 2 log CFU reduction after 20 min cleaning compared

406   to around 4 log CFU with foam. The same trend was observed with hydrophobic spores but at a

407   lesser extent, the use of foam allowing an improvement in detachment efficiency of only 0.5 log in 20

408   min compared to CIP. The variance analysis confirmed that whatever the strains significant

409   differences could be observed between CIP and FFC considering the two kinetics parameters f and

410   k_{max2} (Pr < 0.034 and less than 0.001 respectively), k_{max1} being apparently not significantly modified

411   (Fig. S4 in the Supporting Information).

412   ***3.2.2.   Deposition patterns before and after cleaning***

413   In order to observe whether the different areas of the dried drops were more or less easily

414   removed during the cleaning procedures, the dried deposits were observed before cleaning and after

415   15 seconds and 20 minutes of cleaning. Two different deposition patterns were observed in

416   epifluorescence microscopy (Fig. S4 in the Supporting Information). Whatever the spores, a regular

417   round peripheral ring, often referred to as the "coffee ring" was clearly observed. For Bs PY79 spores,

418   this external coffee ring shape was thick with relatively few adhered spores within the ring.

419   Depending on the trial, the internal deposition was more or less regular, as if the contact line

420   remained fixed or detached and then reattached, resulting in one or more small contaminated areas.

421   Conversely, with the hydrophobic spores Bs PY79 *spsA*, a diffuse peripheral deposit was often

422   observed, within which single spores but also spore clusters are present over the whole surface.

423   After cleaning, the observation of the residual patterns shown a good agreement with the

424   enumeration results (Fig. 8). First, Bs PY79 spores seemed to be removed in a higher extent

425   compared to Bs PY79 *spsA* spores. In the case of Bs PY79 spores after 15 s, the peripheral ring was

426   partially removed by the cleaning procedure and this was particularly noticeable at 13.5 cm/s, but

427   especially at 9 cm/s. After 20 min of cleaning, the ring had completely disappeared at 9 and 13.5

428   cm/s and to a lesser extent at 4.5 cm/s. However, spores were still visible on the inner area of the

429 deposits except for foam after 20 min at 9 cm/s. Regarding the cleaning of Bs PY79 *spsA* spores,

430 spores, and small clusters seemed to be greatly removed while the larger clusters seemed to have

431 better resisted the detachment, and the peripheral ring was partially removed only after 20 min. For

432 both strains, removal was visibly greater with foam flow at 9 cm/s than CIP. At 15 seconds, the

433 cleaning of the deposits of hydrophobic spores Bs PY79 *spsA* seemed to induce a slid of the

434 contamination along the surface in the direction of the flow showing a quite scattered pattern visible

435 with foam flow cleaning and CIP (blue arrows on Fig 8). This sliding phenomenon was absent in the

436 case of hydrophilic spores Bs PY79.

437

438 **4. Discussion**

439

440   Foam has been considered as a non-Newtonian fluid and the Herschel–Bulkley model can predict

441 its flow behavior as previously described (Dallagi et al., 2019). At low shear stress (2.2 Pa) the foam

442 flow behaved as a plug flow in one direction, the velocity of the foam being uniform over the entire

443 section as a 1-Dimensional (1D) flow regime. When the wall shear stress exceeded 4.2 Pa the plug

444 behavior remained only at the top side of the duct (2D flow regime), and at shear stresses greater or

445 equal to 5.9 Pa, the foam became completely sheared (3D flow regime) (Al Saabi et al., 2021). The

446 rheological behavior of foams is controlled by processes that occur within the microstructures such

447 as the rearrangement of bubble size, liquid film, and Plateau borders. A slight modification on the

448 pressure or the shear stress applied could lead to deformation on the foam state. In previous studies

449 on the rheology of emulsion and foam, authors have demonstrated the deformation of the bubble as

450 a function of the capillary number (Llewellin and Manga, 2005). Their results show that as the

451 capillary number increases, bubbles start to deform and the film separating bubbles either thicken or

452 shrink trends to maintain the minimal surface energy. However, this deformation can result in

453 developing anisotropy in foams properties if the capillary number exceeds a critical value which is

454 not the case here: for all studied cases *Ca* was lower than 0.1 and the bubbles remained almost

455 spherical with isotropy of the foam nearly preserved.

456 It should be noted that except for the three foam conditions at 1.5, 3, and 4.5 cm/s obtained

457 using 1, 2, or 3 generators with the same surfactant, flow rate, and air pressure content, the increase

458 of the foam velocity up to 9 and 13.5 cm/s was obtained by increasing the surfactant flow rate and

459 air pressure and content in the foam generators. It was demonstrated that the pressure significantly

460 affects the foam texture, and its stability with a potential change in bubble size distributions, liquid

461 drainage, and bubble coalescence (Al-Qararah et al., 2013), a reduction in the average radius of

462 bubbles was observed with the increase of the pressure. These authors reported that the bubble size

463 decreases with the increasing of the rotation speed up to a certain limit under axial mixing in a

464 Becher. At a rotation lower than 5500 RPM (revolution per minute), the foam remains stable since

465 the air is well homogenized in the surfactant solution. Conversely, above 5500 RPM, because of the

466 saturation of air content, the interactions between bubbles were more numerous which favored

467 their coalescence. Thus, their size increases, resulting in a decrease in interfacial stability. The

468 observation of the foam at the highest velocity (13.5 cm/s) allowed to suggest that the large bubbles

469 are more likely the consequence of a movement inside the foam (3D flow regime) allowing the larger

470 bubbles indeed less dense to rise towards the upper wall rather than a coalescence of the bubbles

471 explained by the high speed of the foam. This behavior was probably enhanced by the fact that the

472 foam is quite wet with a quality β of 0.5.

473 Furthermore, the conductimetry and polarography results (Fig. 4) demonstrated a significant

474 impact of the velocity of the bubbles and their sizes on the fluctuation of the liquid film thickness

475 between bubbles and the top wall and on the local wall shear stress increases significantly between

476 two consecutive bubbles (Plateau borders). These variations would directly affect bacteria present at

477 the surface influencing the removal phenomenon. The displacement of the bubbles leads to sudden

478 increases in the Sherwood number due to shear stress peaks, appearing in a harmonic manner

479 directly related to the bubble passage frequency. Comparing foams at 1.5, 3, and 4.5 cm/s, as the

480   velocity increased, the bubbles became smaller with an F02 of 0.29, 0.36, and 0.44. The frequency of

481   the shear stress increased in parallel from 20 up to 45 Hz while amplitude decreased in agreement

482   with previous works (Tisné et al., 2003). Hence, foam at 9 cm/s having a higher amount of small

483   bubble sizes presented the lowest RFS (RFS of 130 %) with the high frequency (f of 70 Hz) related to

484   the thin liquid film height variation measurements. The peaks of the shear stress were clearly

485   observed at the two ends of the bubbles, the bubble front, and the back. As an example, the wall

486   shear stress value between the bubbles is about 15 Pa while it remains lower than 2 Pa under the

487   bubbles, for foam at 4.5 cm/s. These values corresponded therefore to the maximum and minimum

488   film thickness observed, respectively. In the literature, CFD simulations, as well as experimental

489   studies in two-phase gas-liquid slug flow, e.g. in capillary membranes (Kumari et al., 2018), suggested

490   that the major contribution to the wall shear stress came from the bubbles ends and could be

491   attributed to the Laplace pressure difference caused by the surface tension. (Tisné et al., 2004)

492   revealed that it was possible to relate foam flow study to studies of a long bubble moving in

493   capillaries, and they observed that the bubbles moved as flattened bubbles in a Hele-Shaw cell

494   confirming the localization of the shear stress on the Plateau borders.

495   When compared with spore removal kinetics, parameters in relation to the shear stress and

496   bubble size variations seemed to play a significant role in the cleaning efficiency of foam flow. For

497   both Bs strains, the increase of the mean shear stress roughly leads to an improvement in the

498   cleaning efficiency. However, it was not true for the foam at 13.5 cm/s, which showed a reduction in

499   cleaning efficiency, compared to 9 cm/s. This result suggests that other parameters than the mean

500   shear stress were involved in the FFC efficiency and therefore the variation of the local wall shear

501   stress (WSS) as discussed above in relation to the size and the velocity of the bubbles could play a

502   major role. These results are consistent with previous works in literature. Silva et al. highlighted the

503   significant role of the WSS fluctuation on the cleaning efficiency using pulsed flow (Silva et al., 2021).

504   Results showed that shorter periods promoted higher removal of raw milk cells due to the

505   occurrence of the annular effect and its important frequency. A higher frequency of peaks WSS was

506   needed to make turbulent pulse flow effective to remove tomato deposits (Absi and Azouani, 2018).

507   The authors explained obtained results by the fact that at higher frequency the surfaces are

508   submitted more often to the phenomenon caused by peaks. Hence, as the foam has a higher amount

509   of small bubbles, the contamination will be more subjected to the pick of WSS and perhaps also to

510   the viscous dissipation in the narrow Plateau borders between consecutive bubbles since smaller

511   bubbles possess a higher Laplace pressure.

512   Whatever the FFC conditions, the removal kinetics showed a strong detachment rate at the

513   beginning of the cleaning process (less than 1 min), followed by a second kinetic phase described by

514   a slow detachment rate. Previous works on biofilm removal under CIP (Bénézech and Faille, 2018)

515   and bacteria spores under different foam qualities (Al Saabi et al., 2021) have reported similar

516   observations. Neither the shear stress nor the bubble size has affected the first kinetic phase rate of

517   removal with Bs PY79 spores, while high shear stress induced low k_{max1} with Bs PY79 *spsA*. For both

518   strains, as the shear stress increased, the f parameter increased (the spore population detached

519   more easily). The synergy between high shear stress and small bubbles (foam at 9 cm/s) would

520   explain the highest k_{max2} and a better cleaning efficiency. To prove or disprove this suggestion, a new

521   foam flow condition was produced at 9 cm/s, using a single generator. The air pressure in the

522   generator in this condition was 3 times more than that for the 9 cm/s foam, produced by three

523   parallel generators. As was expected, the mean shear stress was 9.8 Pa, while the bubble size

524   increased (mean diameter of 0.19 mm with a presence of large bubbles (Fig. S5 in the Supporting

525   Information). When comparing the second detachment phases, foam with the smallest bubbles was

526   more efficient for PY79 spores, by 1 log CFU over 20 min. k_{max2} was 1.5 times higher (with 9.8 Pa foam

527   and small bubble size) than that in the alternative condition tested. For *spsA* spores, k_{max2} seems to

528   be similar in these two conditions.

529   According to (Kondjoyan et al., 2009), the role of capillary forces is not negligible and depends on

530   the size of the bubbles and their speed. In (Al Saabi et al., 2021), the detachment of the hydrophilic

531   spores of *Bacillus amyloliquefaciens* 98/7 occurred at bubble velocities of around 3 cm/s and

532   dramatically decreased at 5 cm/s in line with the work of (Kondjoyan et al., 2009), where the greatest

533   detachment rate was observed, as illustrated by high k_{max1} constant rate values. In this work, no

534   visible changes could be seen for the first kinetic phase with the increase in the foam velocity from

535   9.5 up to 13.5 cm/s, but the second kinetic phase showed a significant decrease in the removal

536   efficiency. For hydrophobic particles, according to (Kondjoyan et al., 2009), the detachment rate

537   would start at higher bubble velocities. In this work, the increase in the foam velocity indeed was

538   accompanied by an increase in the detachment efficiency during the first minutes of the foam

539   cleaning, which corresponds to an increase in the f parameter, resulting in a more rapid and efficient

540   spore removal.

541   Other phenomena would occur under the combination of the drainage and the imbibition effects

542   (Fig. 9). It is known that under gravity and capillarity, the liquid flows through drainage networks

543   called Plateau borders. This phenomenon has been demonstrated in previous works (Maestro et al.,

544   2013). Thus, as discussed before, the spores present in the thin liquid film between the bubble and

545   the solid surface are prone to be absorbed within the Plateau borders under the imbibition effect.

546   This mechanism is driven by the capillary forces. Indeed, these Plateau borders have a curvature that

547   creates a capillary under-pressure in the liquid phase. Owing to this pressure difference, the foam

548   was able to absorb the spores (which were in small size,1 µm), just as a sponge would. It has been

549   proven in the literature that the imbibition mechanism was highly dependent on the bubble size,

550   which is the strongest for foam with a smaller bubble size (Maestro et al., 2013; Mensire et al., 2015).

551   On the other hand, such a mechanism could help in understanding the difference in the results

552   obtained by the two strains of spores. Unlike hydrophilic spores which can be easily trapped by the

553   liquid film, absorbed into the Plateau border and then flushed out of the duct, the hydrophobic

554   character of Bs PY79 *spsA* gives spores a strength to oppose the imbibition effect. They mostly

555   remain in the liquid film and then due to bubble fluctuations, some of them are able to re-adhere to

556   the solid surface. To highlight this phenomenon, the ability of hydrophobic spores to adhere to

557   sterile coupons was tested at a distance of around 10 cm downstream of the contaminated area.

558   Whatever the flow conditions, results showed that 1.3% of the detached hydrophobic spores after 20

559   min of cleaning were able to re-adhere to the surface. Comparatively, the re-adhesion of hydrophilic

560   spores was found to be negligible, at less than 0.1% of the detached spores after 20 min. Otherwise,

561   due to the continuous fluctuations of the shear stress and the liquid film thickness induced by the

562   bubble passage, some spores that were strongly attached to the surface were pushed to other

563   locations, thereby causing a sliding phenomenon. This phenomenon was more visible in the case of

564   hydrophobic spores than for hydrophilic ones. This could be explained by the strongly hydrophobic

565   character of Bs PY79 *spsA*. Recently, Schad et al. have shown that foams with small bubble sizes are

566   more efficient in cleaning glass surfaces contaminated with fluorescent oil (Schad et al., 2021). The

567   authors explained the cleaning by an interplay of imbibition, drainage, and wiping mechanisms.

568   Imbibition and drainage of oil into the Plateau borders of foams were found to be the strongest with

569   small bubbles, which is in concordance with our results. However, the wiping mechanism, i.e.,

570   shifting of the contact line between foam, oil and glass was found to be more efficient with unstable

571   foam than with a stable one. This is not surprising since they used static foam. Given similar

572   conditions, unstable foams clearly clean better than stable foams, being continuously in motion and

573   accelerating the re-arrangements of their bubbles with time which leads, as they explained, to

574   violent wiping motions between the foams and the interface. Consequently, these are not

575   completely irrelevant with our work since in our study foams were used in a dynamic form and the

576   movement/flow was imposed, leading to forceful wiping. However, the instability of foam can reduce

577   the cleaning efficiency through the generation of large bubbles (as observed in the case of foam at 9

578   cm/s).

579

580   **5. Conclusion**

581

582   In this study, we analysed the ability of wet foam flow to remove *Bacillus subtilis* spores from

583   dried droplets on stainless steel surfaces. Two strains, *Bs* PY79 and *Bs* PY79 *spsA*, of different

584   hydrophobicity were used. Regardless of the strain, the foam flow showed a better removal capacity

585   than conventional cleaning in place at the same average shear stress. Optimisation and improvement

586   of cleaning efficiency using foam flow requires a quantification of the key parameters, such as bubble

587   size, liquid film thickness and wall shear stress. Analyses obtained from polarography, conductimetry

588   and bubble size quantification have shown that the magnitude and frequency of fluctuations in wall

589   shear stress and liquid film thickness are related to bubble size and flow velocity. These phenomena

590   are most likely to be the cause of spore removal, as described in the literature, although to a lesser

591   extent, for cleaning with liquid solutions. In contrast, with foam, the particularity of fluctuations at

592   the wall (liquid film thickness and shear stress) in relation to the bubble sizes and their velocities,

593   combined with other probable phenomena such as imbibition and drainage of the liquid film within

594   the foam, favours not only the release of contaminants, but also their entrapment. This leads to the

595   conclusion that a combination of high WSS, and the presence of small bubbles (<0.2 mm) indeed

596   improves surface biocontamination cleaning efficiency. Further studies would be interesting to test

597   the ability of this process to clean actual industrial equipment, which is frequently of complex design.

598   Further research could also be carried out into the removal of other types of microbial fouling by

599   these flowing foams, such as into biofilm contaminations developed on the surfaces of materials

600   other than steel, such as polymers, which are sometimes rougher and often more hydrophobic. The

601   implementation of such a foam cleaning technology for CIP cleaning would request an effective foam

602   removal during the rinsing step. Future work could be envisaged to solve this problem using stimuli-

603   responsive surfactants allowing at request a complete disappearance of the foam.

604

613

614

References

Absi, R., Azouani, R., 2018. Toward automatic cleaning of industrial equipment: pulsed flow-induced wall shear stress. Procedia CIRP 78, 359–363. https://doi.org/10.1016/j.procir.2018.10.001

Al Saabi, A., Dallagi, H., Aloui, F., Faille, C., Rauwel, G., Wauquier, L., Bouvier, L., Bénézech, T., 2021. Removal of Bacillus spores from stainless steel pipes by flow foam: Effect of the foam quality and velocity. Journal of Food Engineering 289, 110273. https://doi.org/10.1016/j.jfoodeng.2020.110273

Al-Qararah, A.M., Hjelt, T., Koponen, A., Harlin, A., Ketoja, J.A., 2013. Bubble size and air content of wet fibre foams in axial mixing with macro-instabilities. Colloids and Surfaces A: Physicochemical and Engineering Aspects 436, 1130–1139. https://doi.org/10.1016/j.colsurfa.2013.08.051

Alvarez-Ordonez, A., Coughlan, L.M., Briandet, R., Cotter, P.D., 2019. Biofilms in Food Processing Environments: Challenges and Opportunities. Annu. Rev. Food Sci. Technol. 10, 173–195. https://doi.org/10.1146/annurev-food-032818-121805

Bénézech, T., Faille, C., 2018. Two-phase kinetics of biofilm removal during CIP. Respective roles of mechanical and chemical effects on the detachment of single cells vs cell clusters from a Pseudomonas fluorescens biofilm. Journal of Food Engineering 219, 121–128. https://doi.org/10.1016/j.jfoodeng.2017.09.013

Blel, W., Legentilhomme, P., Bénézech, T., Fayolle, F., 2013. Cleanabilty study of a Scraped Surface Heat Exchanger. Food and Bioproducts Processing 91, 95–102. https://doi.org/10.1016/j.fbp.2012.10.002

Dallagi, H., Al Saabi, A., Faille, C., Benezech, T., Augustin, W., Aloui, F., 2019. CFD Simulations of the Rheological Behavior of Aqueous Foam Flow Through a Half-Sudden Expansion, in: Volume 1: Fluid Mechanics. Presented at the ASME-JSME-KSME 2019 8th Joint Fluids Engineering Conference, American Society of Mechanical Engineers, San Francisco, California, USA, p. V001T01A030. https://doi.org/10.1115/AJKFluids2019-4650

Deleplace, M., Dallagi, H., Dubois, T., Richard, E., Ipatova, A., Bénézech, T., Faille, C., 2021. Structure of deposits formed by drying of droplets contaminated with Bacillus spores determines their resistance to rinsing and cleaning. Journal of Food Engineering 110873. https://doi.org/10.1016/j.jfoodeng.2021.110873

Delmas, G., Jourdan da Silva, N., Pihier, N., Weil, F.-X., Vaillant, V., De Valk, H., 2010. Les toxi-infections alimentaires collectives en France entre 2006 et 2008 6.

Dubois, T., Krzewinski, F., Yamakawa, N., Lemy, C., Hamiot, A., Brunet, L., Lacoste, A.-S., Knirel, Y., Guerardel, Y., Faille, C., 2020. The sps Genes Encode an Original Legionaminic Acid Pathway Required for Crust Assembly in Bacillus subtilis. mBio 11, e01153-20, /mbio/11/4/mBio.01153-20.atom. https://doi.org/10.1128/mBio.01153-20

Faille, C., Lemy, C., Allion-Maurer, A., Zoueshtiagh, F., 2019. Evaluation of the hydrophobic properties of latex microspheres and Bacillus spores. Influence of the particle size on the data obtained by the MATH method (microbial adhesion to hydrocarbons). Colloids and Surfaces B: Biointerfaces 182, 110398. https://doi.org/10.1016/j.colsurfb.2019.110398

Fan, M., Phinney, D.M., Heldman, D.R., 2018. The impact of clean-in-place parameters on rinse water effectiveness and efficiency. Journal of Food Engineering 222, 276–283. https://doi.org/10.1016/j.jfoodeng.2017.11.029

Farag, M.A., Mesak, M.A., Saied, D.B., Ezzelarab, N.M., 2021. Uncovering the dormant food hazards, a review of foodborne microbial spores' detection and inactivation methods with emphasis on their application in the food industry. Trends in Food Science & Technology 107, 252–267. https://doi.org/10.1016/j.tifs.2020.10.037

Ioana, C., Mansour, A., Quinquis, A., Radoi, E., 2007. Le traitement du signal sous Matlab: Pratique et applications, Hermes Science.

Kondjoyan, A., Dessaigne, S., Herry, J.-M., Bellon-Fontaine, M.-N., 2009. Capillary force required to detach micron-sized particles from solid surfaces—Validation with bubbles circulating in

666 water and 2μm-diameter latex spheres. Colloids and Surfaces B: Biointerfaces 73, 276–283.
667 https://doi.org/10.1016/j.colsurfb.2009.05.022

668 Kriegel, A.T., Ducker, W.A., 2019. Removal of Bacteria from Solids by Bubbles: Effect of Solid
669 Wettability, Interaction Geometry, and Liquid–Vapor Interface Velocity. Langmuir 35, 12817–
670 12830. https://doi.org/10.1021/acs.langmuir.9b01941

671 Kumari, S., Kumar, N., Gupta, R., 2018. Effect of gas–liquid ratio on the wall shear stress in slug flow
672 in capillary membranes. Asia-Pac J Chem Eng 13, e2258. https://doi.org/10.1002/apj.2258

673 Li, G., Tang, L., Zhang, X., Dong, J., 2019. A review of factors affecting the efficiency of clean-in-place
674 procedures in closed processing systems. Energy 178, 57–71.
675 https://doi.org/10.1016/j.energy.2019.04.123

676 Llewellin, E.W., Manga, M., 2005. Bubble suspension rheology and implications for conduit flow.
677 Journal of Volcanology and Geothermal Research 143, 205–217.
678 https://doi.org/10.1016/j.jvolgeores.2004.09.018

679 Maestro, A., Drenckhan, W., Rio, E., Höhler, R., 2013. Liquid dispersions under gravity: volume
680 fraction profile and osmotic pressure. Soft Matter 9, 2531.
681 https://doi.org/10.1039/c2sm27668b

682 Mensire, R., Piroird, K., Lorenceau, E., 2015. Capillary imbibition of aqueous foams by miscible and
683 nonmiscible liquids. Phys. Rev. E 92, 053014. https://doi.org/10.1103/PhysRevE.92.053014

684 Mierzejewska, S., Masłowska, S., Piepiórka-Stepuk, J., 2014. Evaluation of the efficiency of removing
685 protein deposits from various surfaces by foam cleaning. Agricultural Engineering 131–137.
686 https://doi.org/10.14654/ir.2014.149.014

687 Mitchell, J.E., 1965. Investigation of wall turbulence using a diffusion-controlled electrode. University
688 of Illinois.

689 Piepiórka-Stepuk, J., Diakun, J., Sterczyńska, M., Kalak, T., Jakubowski, M., 2021. Mathematical
690 modeling and analysis of the interaction of parameters in the clean-in-place procedure
691 during the pre-rinsing stage. Journal of Cleaner Production 297, 126484.
692 https://doi.org/10.1016/j.jclepro.2021.126484

693 Schad, T., Preisig, N., Blunk, D., Piening, H., Drenckhan, W., Stubenrauch, C., 2021. Less is more:
694 Unstable foams clean better than stable foams. Journal of Colloid and Interface Science 590,
695 311–320. https://doi.org/10.1016/j.jcis.2021.01.048

696 Silva, L.D., Filho, U.C., Naves, E.A.A., Gedraite, R., 2021. Pulsed flow in clean-in-place sanitization to
697 improve hygiene and energy savings in dairy industry. J Food Process Eng 44.
698 https://doi.org/10.1111/jfpe.13590

699 Tisné, P., Aloui, F., Doubliez, L., 2003. Analysis of wall shear stress in wet foam flows using the
700 electrochemical method. International Journal of Multiphase Flow 29, 841–854.
701 https://doi.org/10.1016/S0301-9322(03)00038-7

702 Tisné, P., Doubliez, L., Aloui, F., 2004. Determination of the slip layer thickness for a wet foam flow.
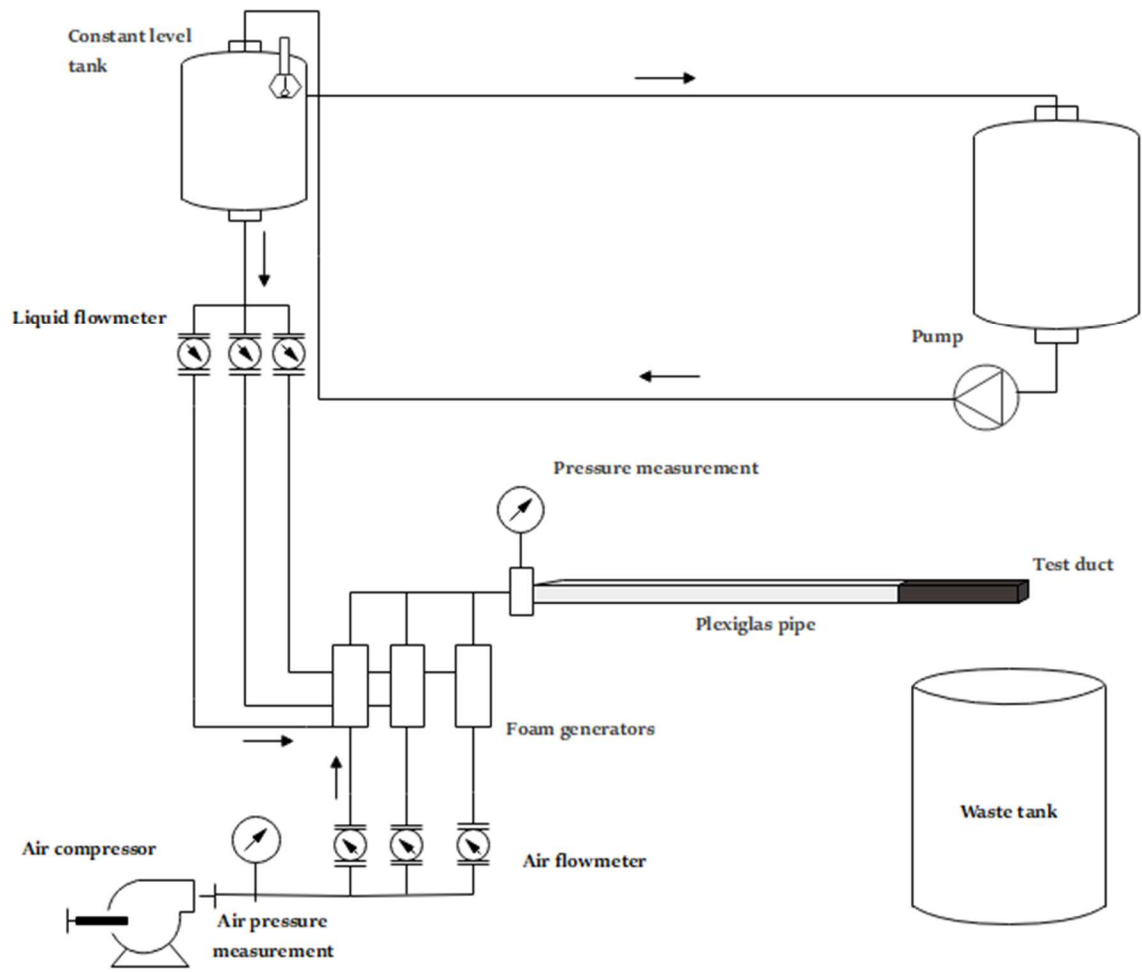703 Colloids and Surfaces A: Physicochemical and Engineering Aspects 246, 21–29.
704 https://doi.org/10.1016/j.colsurfa.2004.07.014

705

706

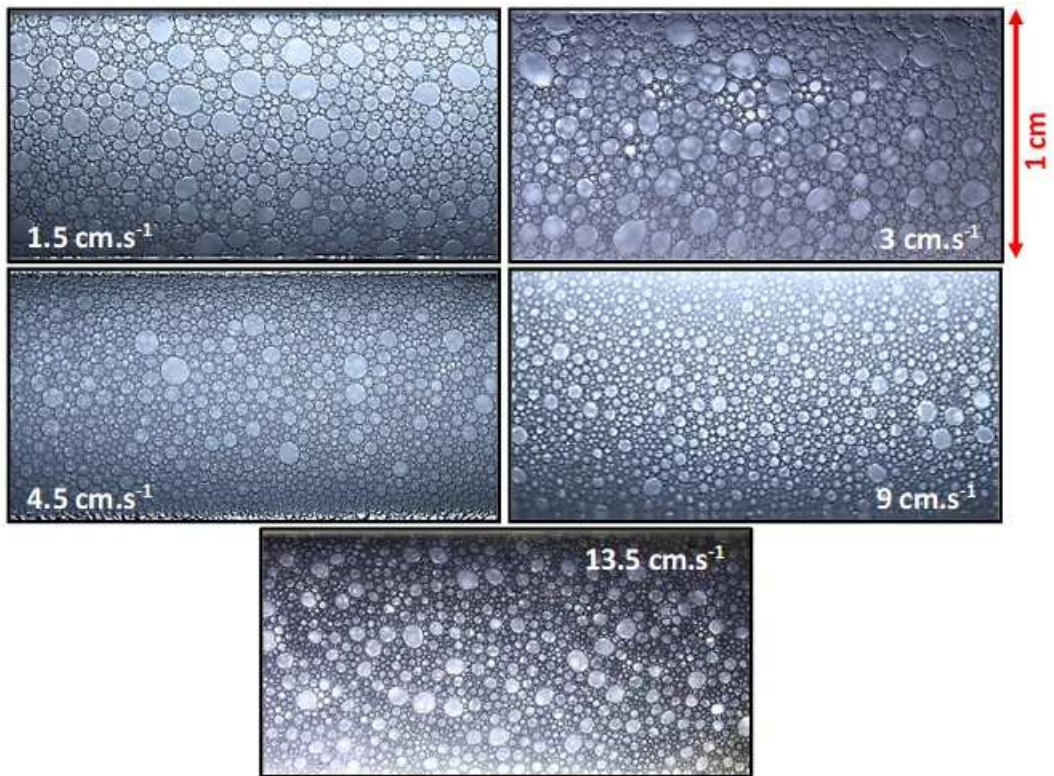**Fig. 1.** Experimental set-up for studying the foam cleaning in place process.

Fig. 2. Top view of foam at the wall of the transparent pipe (the entire width, 1 cm) for the different foam flow conditions.
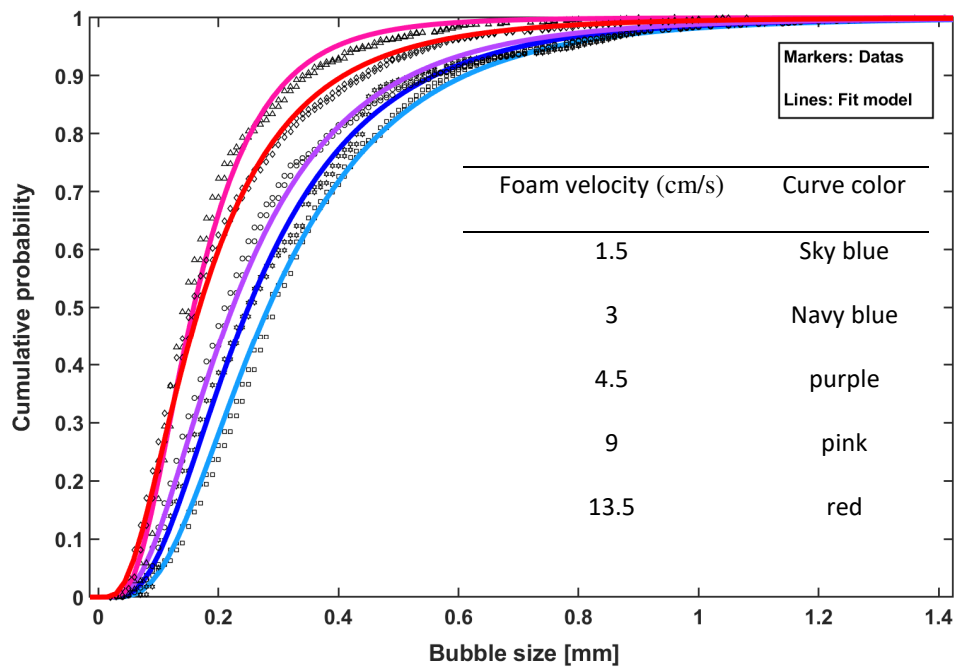
Fig. 3. Cumulative fraction of the bubble size distribution for all the foam flow conditions. The markers present the brut data and the lines represent the Lognormal model fitted to each condition.
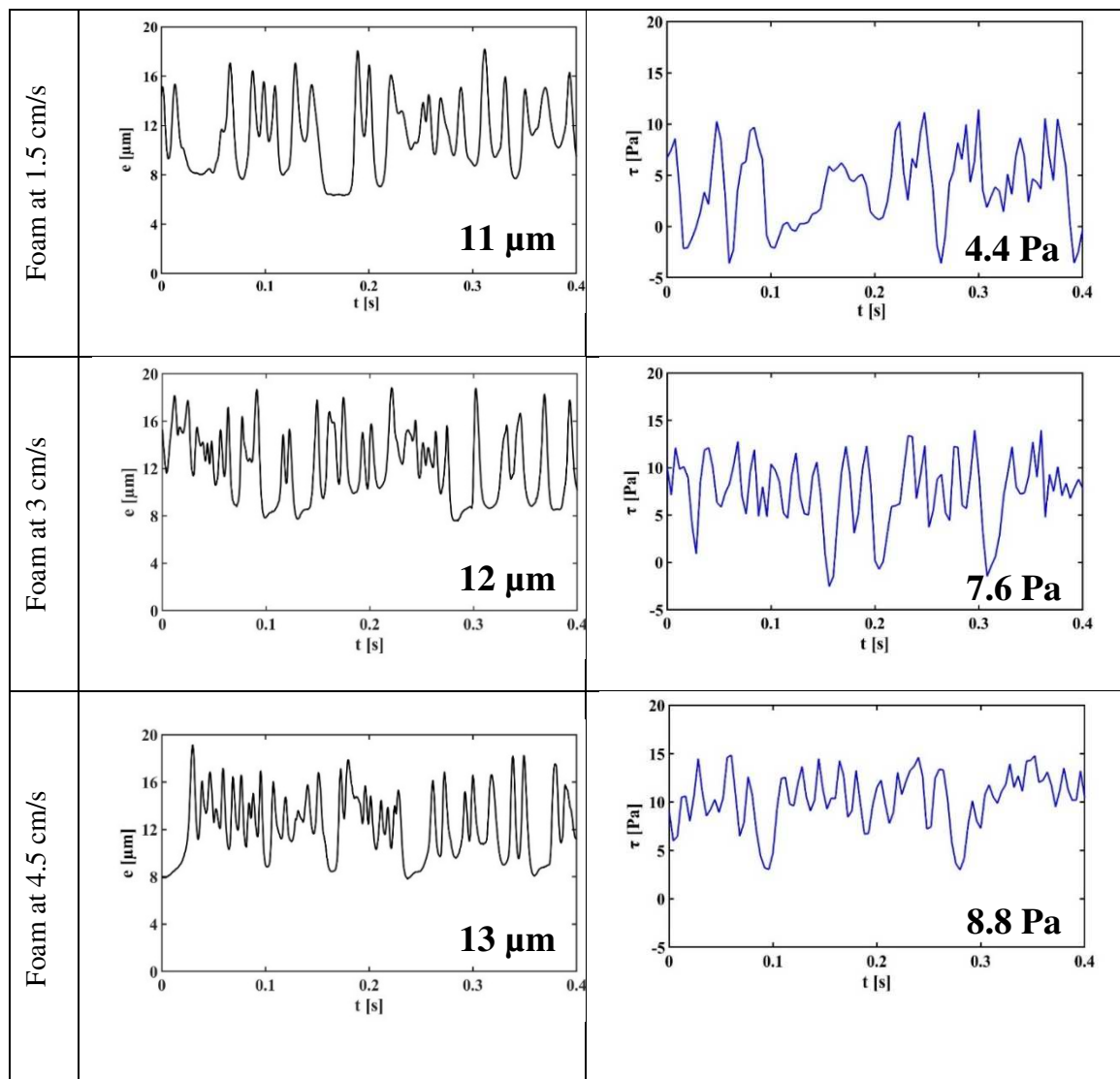
Fig. 4. Example of the evolution of wall film thickness (left) and wall shear stress (right) given by the temporal signals of conductimetry and polarography over the top wall for the three cases, respectively. The values indicated in the images show the mean thickness and the mean wall shear stress during 40 seconds of acquisition.
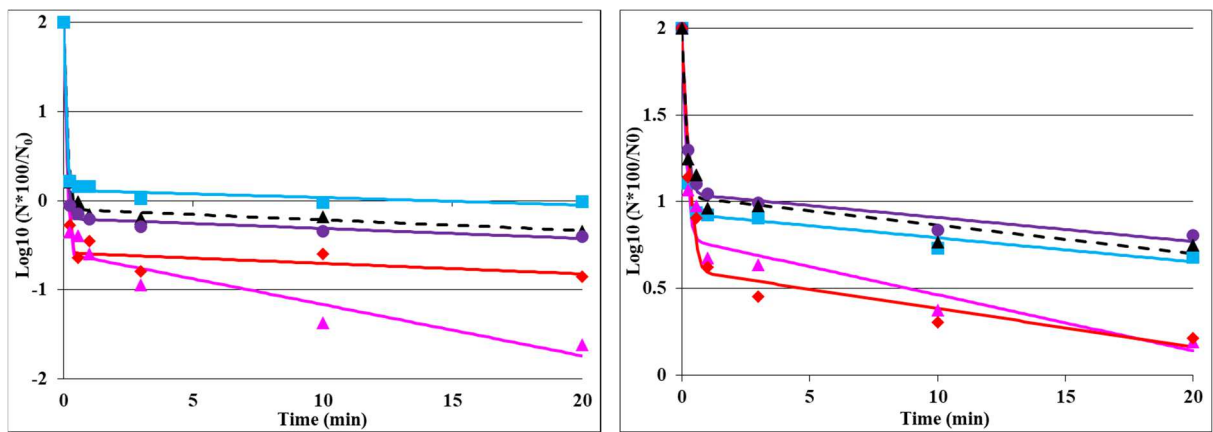
Fig. 5. Removal kinetics of *B. subtilis* PY79 (left) and *B. subtilis* PY79 *spsA* spores under the different flow conditions. Markers showed the data of three repetitions, and the line represents the biphasic fitted model fit to each condition: 1.5 cm/s (sky square), 4.5 cm/s (purple circle), 9 cm/s (pink triangle), 13.5 cm/s (red diamond), and CIP (black triangle).
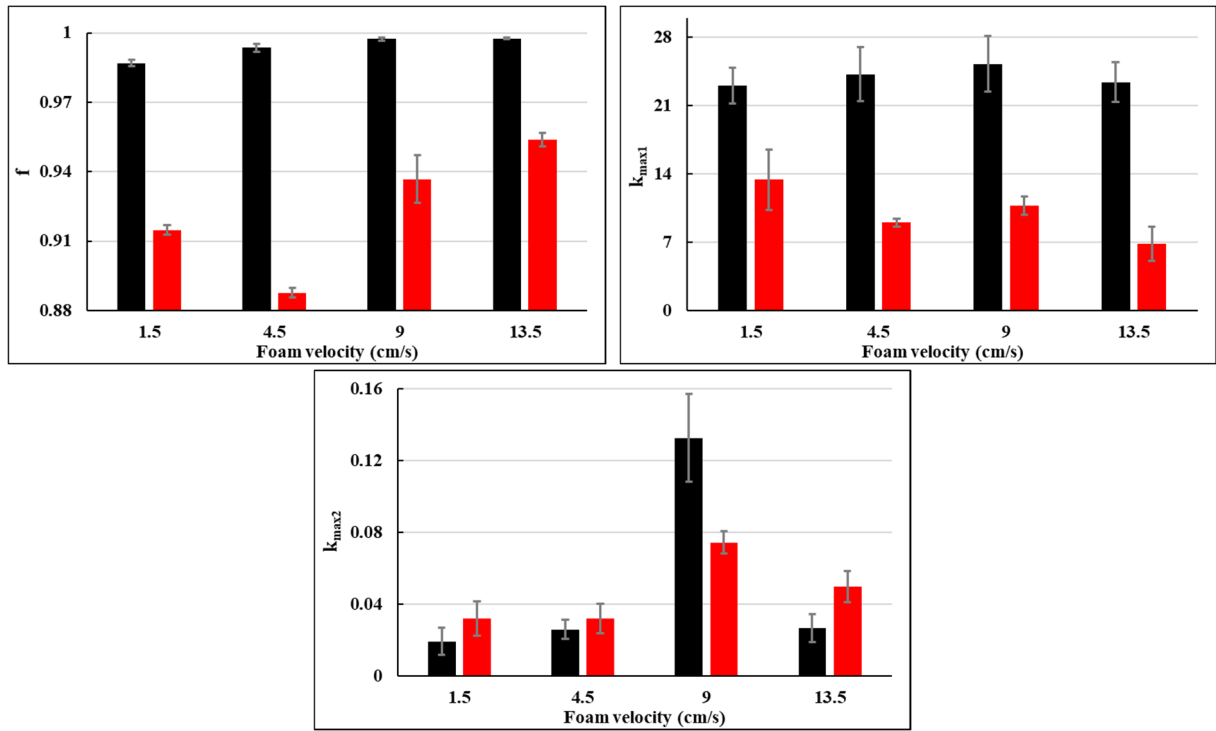
Fig. 6. kinetics parameters f, K_{max1}, and K_{max2} for Bs PY79 (black color) and Bs PY79 *spsA* (red color) spores under different flow conditions.
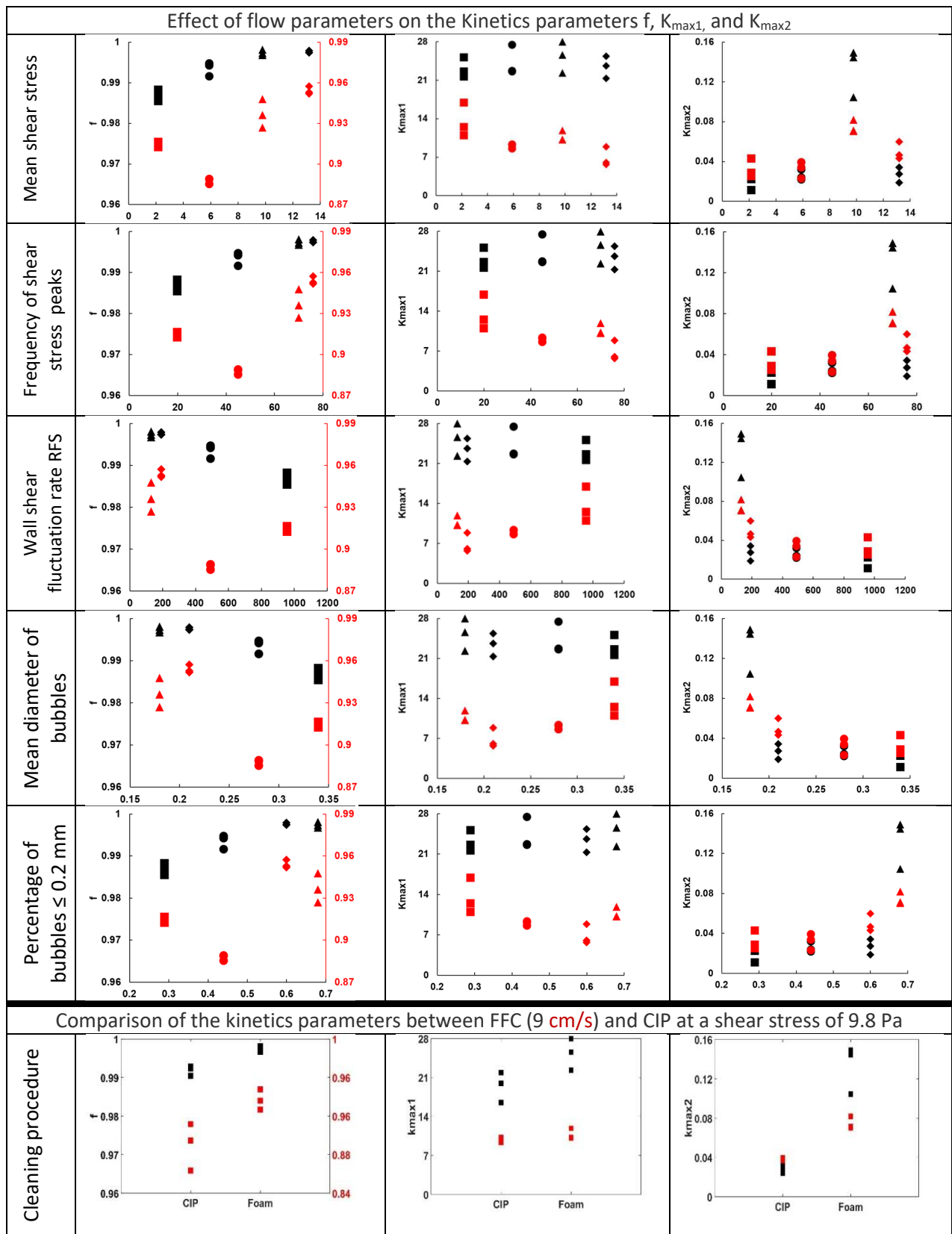
Fig. 7: Variations induced on the kinetics parameters f, K_{max1} and K_{max2} for Bs PY79 (black color) and Bs PY79 *spsA* (red color) spores under different flow conditions: 1.5 cm/s (square), 4.5 cm/s (circle), 9 cm/s (triangle), 13.5 cm/s (diamond), and CIP.
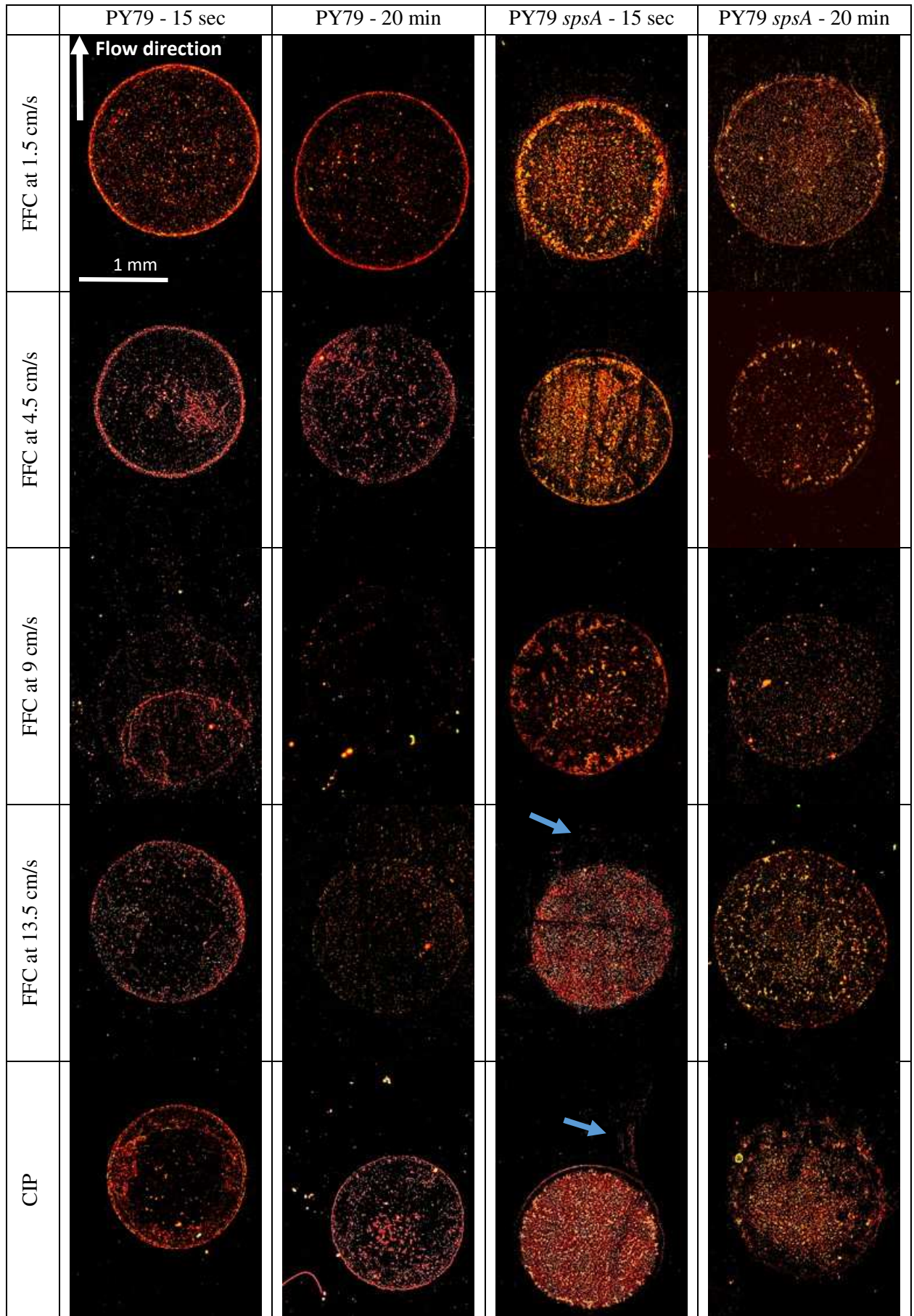
| | PY79 - 15 sec | PY79 - 20 min | PY79 *spsA* - 15 sec | PY79 *spsA* - 20 min |

Fig. 8: Residual deposition patterns of droplet contaminated with Bs spores after complete evaporation and further subjected to 5 seconds and 20 minutes of FFC and CIP procedures, examined by epifluorescence with a Zeiss Axioskop 2 plus microscope (x50). Blue arrows indicated the sliding of the spores observed at 15 s for Bs PY79 *spsA.*
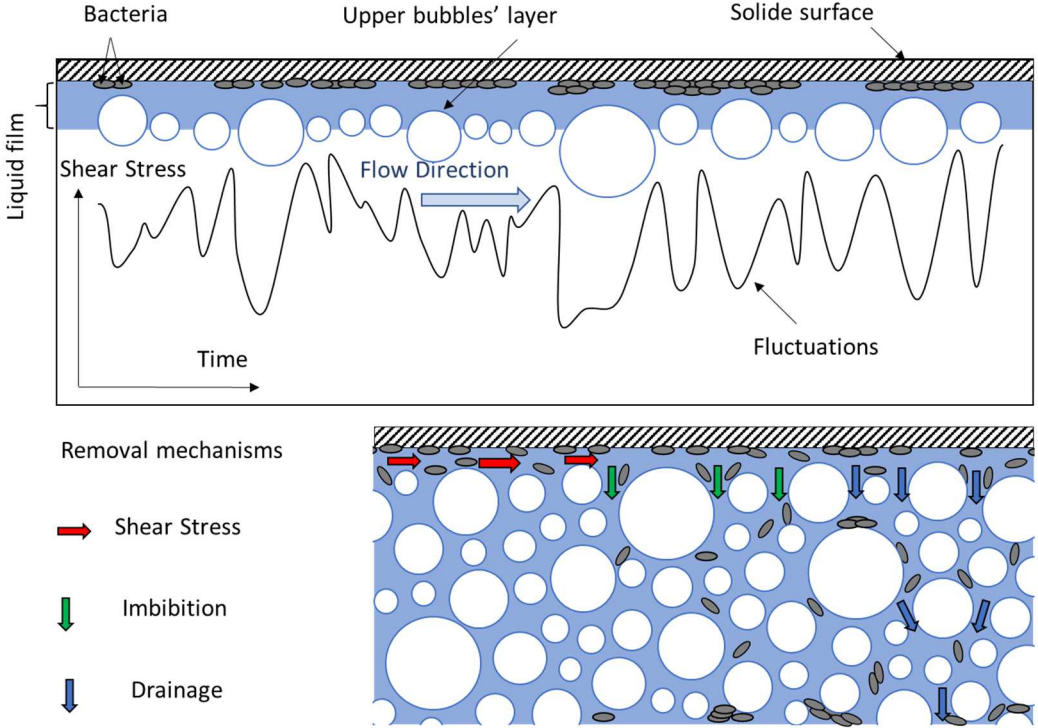

Fig. 9: Schematic of the suggested cleaning mechanisms using foam flow

Table 1: Description of the different flow conditions carried out. The FFC and CIP represent the foam flow conditions and the cleaning-in-place that has been processed for removal of Bacillus spores from stainless steel surfaces, respectively.

Flow conditions	u (cm.s^{-1})	Ca [10^{-3}]	τ (Pa)	Dmean (mm)	F005	F02	RFS (%)	f (Hz)
FFC	1.5	0. 5	2.2	0.34	0.002	0.29	957	20
	3	1.1	4.2	0.30	0.006	0.36	688	39
	4.5	1.6	5.9	0.28	0.013	0.44	491	45
	9	3.3	9.8	0.18	0.022	0.68	130	70
	13.5	4.8	13.2	0.21	0.043	0.60	193	76
CIP	180	----	10	-------------				

Table 2: Tuckey grouping for PY79 and *spsA* spores. According to the Tukey grouping, letters were indicated with potentially three classes A, AB, B, C and D depending on the parameter: common letters meaning no significant differences.

Mean Velocity of FFC conditions	f		Kmax1		Kmax2	
	PY79	*spsA*	PY79	*spsA*	PY79	*spsA*
1.5 cm/s	C	C	A	A	B	B
4.5 cm/s	B	D	A	AB	B	B
9 cm/s	A	B	A	AB	A	A
13.5 cm/s	A	A	A	B	B	B